frontiers | Frontiers in Earth Science

TYPE Original Research
PUBLISHED 06 March 2023
DOI 10.3389/feart.2023.1140326

OPEN ACCESS

EDITED BY
Hu Wang,
Southwest Jiaotong University, China

REVIEWED BY
Wenjun Zheng,
School of Earth Sciences and Engineering, Sun Yat-sen University, China
Chuanyong Wu,
Institute of Disaster Prevention, China
Daoyang Yuan,
Lanzhou University, China
Jun Shen,
Institute of Disaster Prevention, China

*CORRESPONDENCE
Lichun Chen,
glutclc@glut.edu.cn

SPECIALTY SECTION
This article was submitted to Structural Geology and Tectonics, a section of the journal Frontiers in Earth Science

RECEIVED 08 January 2023
ACCEPTED 17 February 2023
PUBLISHED 06 March 2023

CITATION
Feng J, Chen L, Han M, Gao S, Li Y, Lu L and Chen S (2023), Multi-fault rupture behavior of the 1786 *M* $7^3/_4$ Kangding earthquake on the eastern margin of the Tibetan Plateau.
Front. Earth Sci. 11:1140326.
doi: 10.3389/feart.2023.1140326

Multi-fault rupture behavior of the 1786 *M* $7^3/_4$ Kangding earthquake on the eastern margin of the Tibetan Plateau

Jiahui Feng[1], Lichun Chen[2]*, Mingming Han[3], Shuaipo Gao[4], Yanbao Li[1], Lili Lu[1] and Shunyun Chen[1]

[1]State Key Laboratory of Earthquake Dynamics, Institute of Geology, China Earthquake Administration, Beijing, China, [2]College of Earth Sciences, Guilin University of Technology, Guilin, China, [3]Chengdu Center of China Geological Survey, Chengdu, China, [4]College of Earth Sciences and Engineering, Hebei University of Engineering, Handan, China

The 2022 Luding *Ms* 6.8 earthquake has drawn attention to the Xianshuihe fault zone. Historically, there was an *M* $7^3/_4$ earthquake in this region in 1786. Because the surface rupture of this historic earthquake was not obvious, there is still much debate over the extent of the surface rupture, which is critical for comprehending tectonic activity and assessing seismic risk for the Xianshuihe fault (XSHF). In particular, the seismogenic structure of this earthquake was connected by three active left-lateral strike-slip faults—the Anninghe fault (ANHF), Daliangshan fault (DLSF), and XSHF—where a large earthquake could cause multi-fault rupture. Given these criteria, we report the results of a series of trenches excavated in the vicinity of the epicenter at the northern section of the DLSF, the northern section of the ANHF, the Zheduotang section, and the Selaha section of the XSHF. We find that 1) three palaeoseismic events have been revealed on the northern section of the ANHF: BE1, ~1003 AD; BE2, 1000–1182 AD; and BE3, 1536 AD as *M* 7 earthquakes, and 2) two palaeoseismic events have occurred on the Selaha fault during the last 500 years. The first event corresponds to the AD 1725 Kangding *M* 7 earthquake, and the latest event may be the AD 1786 *M* $7^3/_4$ earthquake. 3) Three palaeoseismic events occurred on Zheduotang: ZD1, 1215 BC~315 AD; ZD2, 830 BC~705 AD; and ZD3, the 1955 AD Kangding *M* $7^1/_2$ earthquake. 4) The 1786 Kangding *M* $7^3/_4$ earthquake was probably a multi-fault rupture event, as evidenced by the trenching profile evidence, nearby offset geomorphic features, and historical earthquake data. Not only the Moxi fault, a seismogenic structure, but also the southern end of the Selaha fault to the north and the Shimian fault (DLSF) to the south simultaneously broke during this earthquake.

KEYWORDS

1786 Kangding earthquake, Xianshuihe fault, palaeoearthquake, multi-fault rupture, complex seismogenic structure

1 Introduction

Large earthquakes typically occur at the ends of faults or in the region where the fault strike changes (Gkarlaouni et al., 2008; Lozos et al., 2017). The Kangding–Shimian area's structural node is where the Longmenshan fault (LMSF), Xianshuihe fault (XSHF), Anninghe fault (ANHF), and Daliangshan fault (DLSF) all converge, making the area's structural features more complicated and

prone to earthquakes. The epicenter of the 5 September 2022, Luding *M* 6.8 earthquake was located near Moxi township, Kangding. Twenty-five individuals remain missing, and ninety-three people died in this earthquake. In 1786 AD, the Kangding *M* $7^3/_4$ earthquake also struck this region. Because the surface rupture of the earthquake has vanished since it occurred more than 200 years ago, there is still controversy about the distribution of the surface rupture. Some studies have suggested that the surface rupture of the 1786 Kangding *M* $7^3/_4$ earthquake was distributed in the Moxi–Selaha segment of the XSHF (Li, 1997; Wen et al., 2008). According to the most recent mapping data, the seismogenic structure of this earthquake is the southern section of the XSHF, and the surface rupture was located between Kangding and Tianwan (Chen et al., 2011, 2016), with a rupture length of approximately 80 km. Generally, it is thought that Kangding is the segmented boundary of the Moxi segment and the central segment (Selaha segment) of the XSHF (An, 2010). The beginning and end positions of an earthquake's surface rupture are determined by the segmentation boundary of the fault, which has an impact on how strain is accumulated and distributed on the fault as well as how large earthquakes rupture. Recent studies on multi-fault ruptures have altered the previous understanding of fault activity segmentation boundaries (Fletcher et al., 2014; Stirlinghv et al., 2017; Hamling et al., 2017; Chen et al., 2018). The three branches of the Huiyuansi–Kangding segment and the Moxi segment along the XSHF, as well as the ANHF, are seismogenic in their own right (Liang et al., 2020; Ma et al., 2022) and have also experienced *M*>7 earthquakes throughout history. However, some researchers believe that the

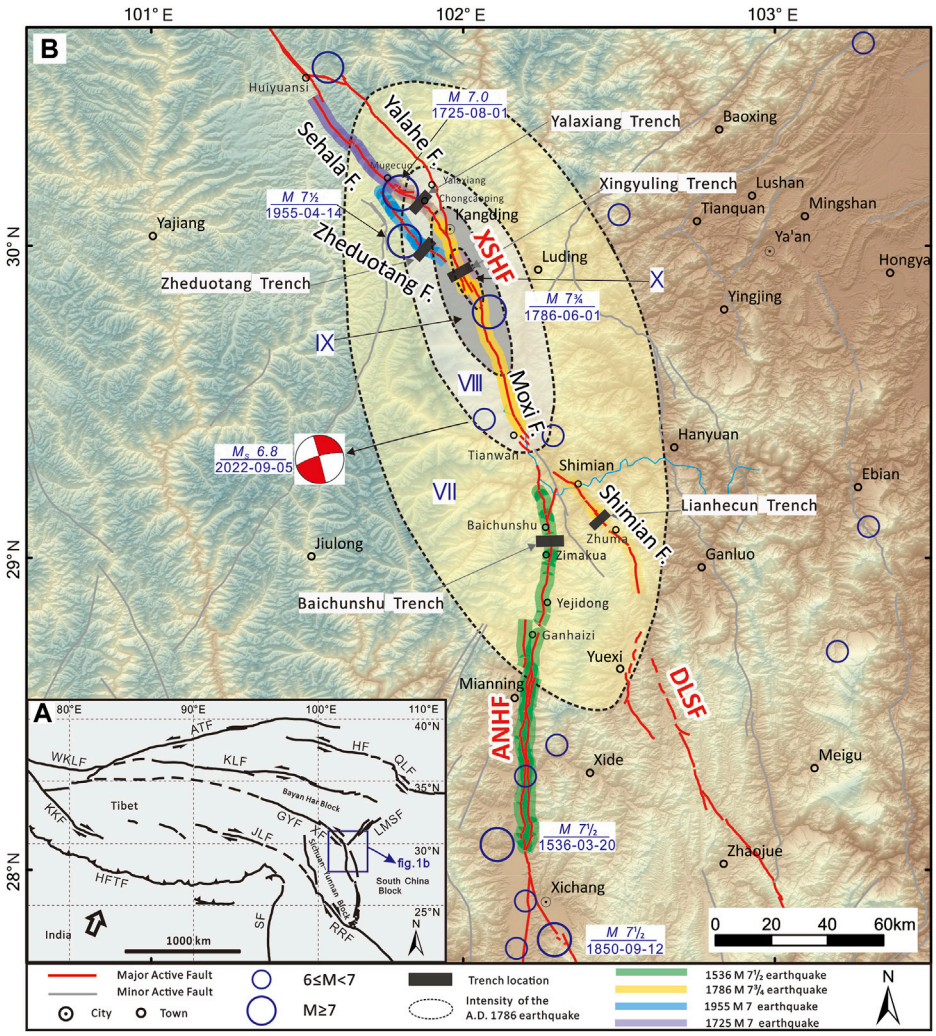

FIGURE 1
Regional tectonics and seismicity in south-eastern Tibet. **(A)** Geotectonics of the study area. **(B)** Characteristics of seismicity in the study area. The blue rectangle in Figures 1A indicates the study area located at the boundary of the Bayan Har block, Sichuan–Yunnan block, and South China block. The blue circles of different sizes indicate epicenters of earlier documented historical earthquakes (Department of Earthquake Disaster Prevention, 1995; Department of Earthquake Disaster Prevention, 1999). Dotted lines indicate the intensity map of the 1786 AD earthquake (Gu, 1983; Wang and Pei, 1998). The bands of different colors represent the surface rupture range of historical earthquakes: the rupture extent of the 1536 AD earthquake obtained from Wang et al. (2014) and Ran et al. (2008a); the rupture extent of the 1786 AD earthquake obtained from Wang and Pei (1998) and Chen et al. (2011); the rupture extent of the 1955 AD earthquake obtained from Zhou et al. (2001a); and the rupture extent of the 1725 AD earthquake obtained from Han et al. (2022). The Hillshade map is generated from the Advanced Spaceborne Thermal Emission and Reflection Radiometer (ASTER) Global Digital Elevation Model (ASTGTM) (90-m resolution). Abbreviations of the active faults: ATF, Altyn Tagh fault; HF, Haiyuan fault; XF/XSHF, Xianshuihe fault; JLF, Jiali fault; RRF, Red River fault; BLF, LMSF, Longmenshan fault; DLSF, Daliangshan fault; ANHF, Anninghe fault; and ZMHF, Zemuhe fault.

Huiyuansi–Kangding segment's three secondary faults are integrated into the deep crust and have a unified fault surface, which means that these three faults exhibit the tail effect of deep fracture dislocation on the surface (Zhou et al., 2001a). This structure appears to indicate that multiple faults could rupture simultaneously in the southern segment of the XSHF fault and the northern segment of the ANHF and DLSF. Based on previous trenching work, we have excavated several trenches in the northern segment of the DLSF, the northern segment of the ANHF, and the Zheduotang and Selaha segments of the XSHF. In addition to exploring the rupture range of the 1786 Kangding earthquake, we aim to expose and contrast the (previous) earthquake rupture events of these faults which can also provide new basic data for understanding and evaluating the future seismic risk in the Shimian–Kangding area.

2 Regional seismotectonic setting

The study area, located at the boundary of the Bayan Har block, the Sichuan–Yunnan block, and the South China block (Deng et al., 2002; Zhang et al., 2003), is connected by three active left-lateral strike-slip faults, the ANHF, DLSF, and XSHF (Figure 1B). The XSHF shows a NE-trending protruding arc in a plane shape, which can be roughly divided into three major geometric segments bordered by the Qianning Basin and Kangding County, known as the NW segment, middle segment, and SE segment (Long and Deng, 1986; Li, 1997; Wen, 2000; Wen et al., 2008; An, 2010).

The middle segment of the XSHF has a complicated geometric structure. This segment separates into three secondary faults—the Yalahe fault, the Selaha fault, and the Zheduotang fault—between the southern Huiyuansi Basin and southern Kangding. The three secondary faults have historically experienced earthquakes of $M \geq 7$ (Liang et al., 2020; Ma et al., 2022). The Selaha fault is the seismogenic structure for the 1725 Kangding M 7 earthquake, and the surface rupture of this earthquake can still be seen (Han et al., 2022; Long & Deng, 1986). The Yalahe fault may have been the source of the 1700 North Kangding M 7 earthquake (Liang et al., 2020). An M 7 earthquake struck the Zheduotang fault in 1955 (Zhou et al., 2001a; Wen et al., 2008).

The south-eastern portion of the XSHF (Moxi Segment) is distributed from Kangding to Shimian. The Moxi segment's surface morphology consists of a single structure with a straightforward form. The most widespread and damaging earthquake ever recorded in the XSHF's history was the South Kangding M $7^3/_4$ earthquake that struck the Moxi region in 1786 (Chen et al., 2011; Chen et al., 2016).

Although various researchers have obtained varied findings about the late Quaternary activity rate of each segment of the XSHF, the overall trend indicates that the southeast segment's late Quaternary activity rate is approximately 6–10 mm/a, and the center segment's late Quaternary activity rate is typically 3–8 mm/a (Qian et al., 1988; Zhao et al., 1990; Allen et al., 1991; Li, 1997; Zhou et al., 2001b; Xu et al., 2003; Wen et al., 2008; Chen, 2006).

The ANHF was divided into two segments by Mianning (Ran et al., 2008a). The results of the field investigation indicate that the left-strike slip rate of the northern segment of the ANHF is 3.6–4.0 mm/a, while the southern segment's slip rate since the Holocene is approximately 4.4–6.5 ± 1 mm/a (Wang et al., 2018; Xu et al., 2003), and the Xichang earthquake of magnitude M $7^1/_2$ occurred on the ANHF fault in 1536 AD (Ran et al., 2008b; Wang et al., 2014).

The DLSF is a structural belt with a total width of approximately 15 km, consisting of six secondary faults (He et al., 2008). The Gongyihai fault and the Shimian fault make up the northern segment (Institute of Geology, CEA, 2019). Since the late Pleistocene, the Gongyihai fault has been a weakly active fault according to the most recent geological and geomorphological surveys. High-precision geomorphological observations and satellite interpretation indicate that the late Quaternary left-strike rate of the Shimian fault is 1.5–3.3 mm/a, which is consistent with the fault's relatively intense late Quaternary activity (Sun et al., 2015). Although the DLSF lacks historical earthquake records, palaeoearthquake research has shown evidence of intense seismic activity, indicating that earthquakes of M 7 or above have occurred and will occur in the future (Gao et al., 2016; Sun et al., 2019; Feng et al., 2021).

3 Methods

Generally, earthquakes with a magnitude greater than M $6^3/_4$ will produce surface rupture (Deng et al., 1992). The surface rupture traces of large earthquakes in geological records can be revealed according to the palaeoearthquake research (Ran et al., 2012a; 2012b). Based on the comparative analysis of palaeoearthquakes in different locations, the rupture range of historical earthquakes can be found, and then, the rupture mode of faults can be clarified (Scharer et al., 2017; Onderdonk. et al., 2018; Yuan, 2018; Wang et al., 2018). In this regard, to explore the rupture range of the 1786 earthquake, we excavated four trenches in the vicinity of the 1786 earthquake epicenter in the northern section of the DLSF, the northern section of the ANHF, the Zheduotang section, and the Selaha section of the XSHF.

3.1 Trench excavation and identification of palaeoearthquakes

To investigate palaeoearthquakes along the strike-slip faults in the Sichuan–Yunnan area, fault troughs and sag-ponds are emerging as the best trench sites (Ran et al., 2012a). We have chosen four trenching sites that favor fine-grained deposits. During excavation, trenches were required to be 2.5 m deep and 2.5 m wide, and each wall was virtually vertically excavated and then meticulously cleaned, gridded in squares of 1×1 m, photographed, and printed for thorough field mapping. According to Ran et al. (2012a, 2012b), the main criteria for identifying strike-slip fault palaeoearthquake events with strike-slip faults can be summarized as follows: sedimentary sequence characteristics (such as sedimentary evolution and sedimentary interruption), the relationship between faults and strata, strata deformations (such as bending and dislocation), tension-filled wedges, and infilled and void fissures.

3.2 Radiocarbon dating

In all trenches, several radiocarbon samples were taken from both faulted and unfaulted strata. These samples came from organic

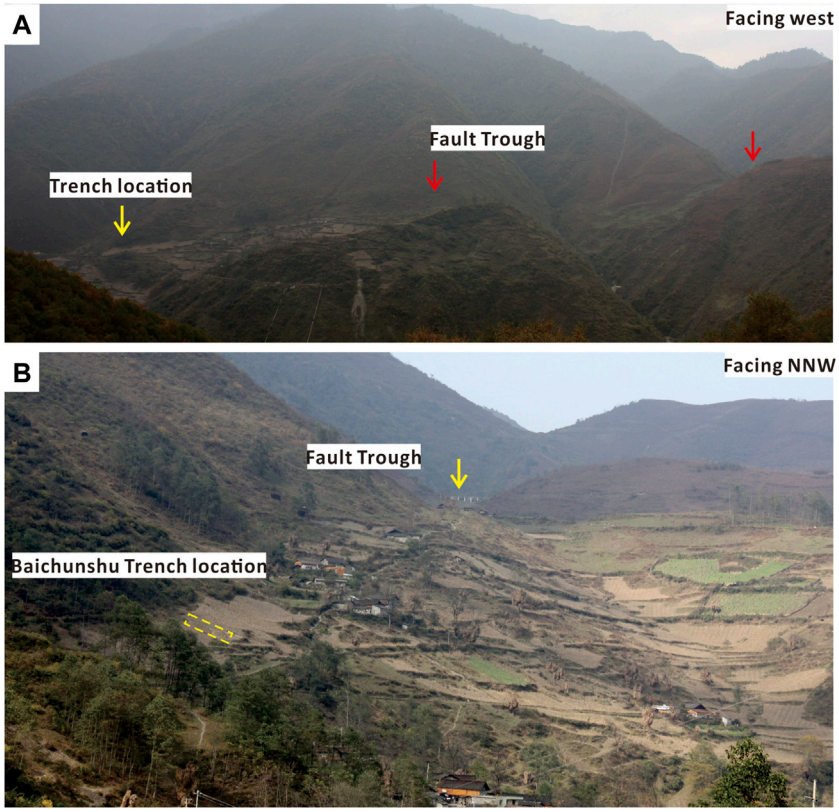

FIGURE 2
Fault geomorphology and trench layout in Baichunshu. **(A)** Field photo of the faulted landforms around trench. **(B)** Local enlarged photograph of **(A)**.

sediment, wood, and charcoal, which have all been advocated as excellent sources for determining the sedimentation age of stratigraphic units. All samples were sent to Beta Analytic, Inc., United States, for accelerometer mass spectrometer dating. Using the OxCal 4.4 technique procedure (Ramsey, 2009; Reimer et al., 2013), the sample ages were adjusted to two-sigma calendar ages (95.4% confidence interval).

4 Palaeoearthquake investigation

4.1 Baichunshu trench

Evident fault activity indications and micro landforms, including fault troughs, steep ridges, fault ponds, and abandoned gullies, were found along the northern section of the ANHF in the region from Ganhaizi to Shimian County. The linear image characteristics of fault activity in the late Quaternary are particularly obvious close to Baichunshu village, with a linear distribution of fault troughs and slope trough landforms (Figure 2). The trench was excavated at a slope trough approximately 1 km north of Baichunshu village, and the valley topography favors continuous deposition with fine-grain deposits carried by a hillside stream (Figure 2B). The trench profile reveals that the underlying materials are mostly clay materials of static water accumulation or faulted ponds, as opposed to the overlying materials, which are primarily sand gravels of deluvial facies (Figure 3). Based on the differences in composition, structure, color, and sedimentary facies, these clays and gravel layers are divided into five units, including six subunits (Table 1).

By analyzing the deformation evidence revealed by the Baichunshu trench, two faults can be identified. On the eastern wall, the fault events are clear. Unfortunately, the timing of palaeoseismic events in Table 1 cannot be well constrained due to the absence of sedimentary sequences. On the western wall, faulted events are also very clear (Figure 3). According to the relationship between stratigraphic characteristics and faulted deformation, three palaeoseismic events were revealed, namely, BE1, BE2, and BE3, from the oldest to youngest.

The BE1 event occurred before U3b and after U2c. The main evidence is as follows: ①F2-1 faulted layer U2-1 (Figure 3); ②sedimentary facies had changed after U2c; U3b, which is only distributed on the west side of the profile, is the hydrostatic sedimentary environment, with sag-pond sedimentary characteristics, while the U2c layer is deluvial facies with the continental sedimentary environment.

The BE2 event occurred after U3b and before U4a. The main evidence is as follows: ①sedimentary facies had changed after U3b; ②there are differences in the deformation degree—the dragging deformation of U3b is very strong, while the deformation of U4,

10.3389/feart.2023.1140326

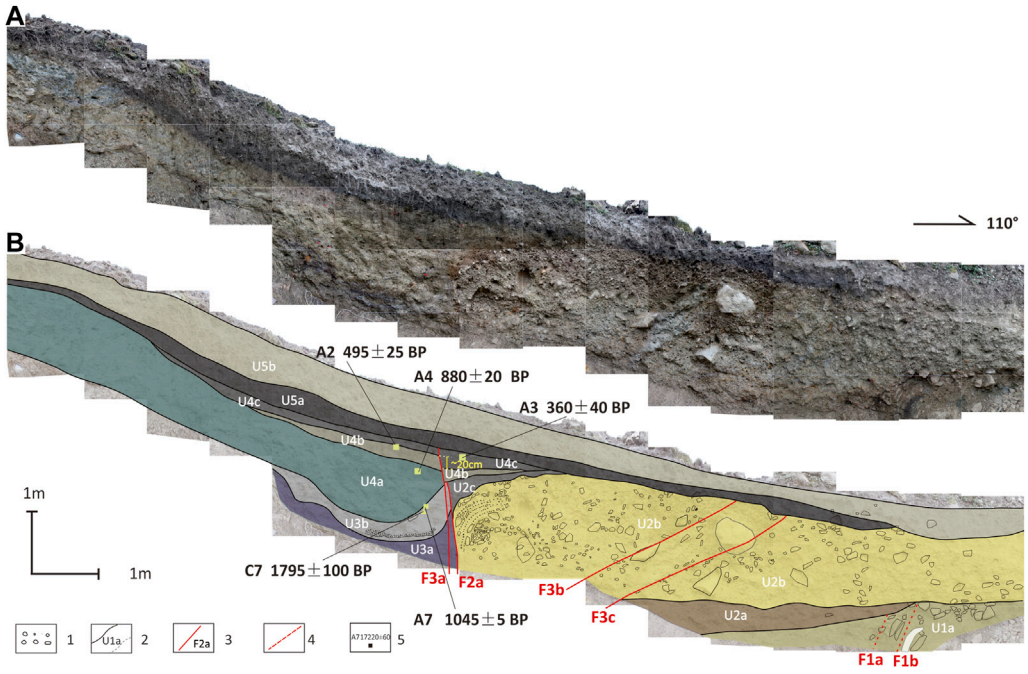

FIGURE 3
Photographic mosaic (upper) and interpretation log(lower) of the Baichunshu trench. **(A)** Photographic mosaic of the north wall of the trench; **(B)** interpretation log(lower) of the trench. 1) Gravel; 2) depositional unit sequence and stratigraphic boundary (dotted line indicates the unclear boundary); 3) fault trace; 4) speculate fault; and 5) location and dating of ^{14}C samples.

TABLE 1 Units and descriptions exposed by the Baichunshu trench.

Unit	Description
U1	The yellow–brown slightly gray gravel layer, the gravel particle size is large, ranging from 1 cm to 20 cm, the sorting is poor, and it is an alluvial accumulation
U2	A clay gravel layer containing siltier gravel, which is slope sediment. It can be divided into three sublayers, U2a is a brownish-yellow slope flood gravel layer, the gravel diameter is less, there is a certain rounding, and the boundary with the lower strata is clear, and it is stacked before the ridge; U2b is a mixture of bluish-gray gravel and clay, containing boulders; U2C is a brownish-red gravel-bearing clay layer
U3	Gray gravel-bearing clay layer with clear boundaries from the upper and lower strata. According to the gravel content, it can be divided into two sublayers, U3a is a gray gravel clay layer; U3b is a blue–gray carbon-containing silt layer and clay layer, and the top is partially laminated carbon chips and carbon mud, and the carbon AMS dating result obtained in this layer is 1045 ± 5 BP.
U4	Pale yellow clay layer, which can be divided into three sublayers according to color and sedimentary characteristics, U4a is an earthy yellow gravel-bearing fast clay layer, and the carbon-like AMS dating result is 880 ± 20 BP; U4b is a light earthy yellow clay layer, and the carbon-like AMS dating result is 495 ± 25 BP; U4c is an earthy yellow clay layer, and the carbon AMS dating result is 360 ± 40 BP.
U5	The surface clay layer, which has a clear stratigraphic boundary with the underlying stratigraphy, showing unintegrated contact, and the U5a layer is a gray–black clay layer; U5b is a surface tillage soil layer
U5	Gray–black topsoil layer rich in plant roots, containing a small amount of small gravel particles. Some large gravel particles are only visible near the fault at the northern end of the eastern wall

especially the upper part U4b and U4c, is weaker, and the dislocation of U4b is only 20 cm.

The BE3 event occurred between U4c and U5a, and the main evidence is that U5a was not faulted and deformed, while U4c was dislocated by F3-1.

At the 95.4% confidence interval (Table 4), the calendar ages of the three events from OxCal 4.4 are as follows: Event BE1, ~1003 AD; Event BE2, 1000–1182 AD; and Event BE3, after 1535 AD.

4.2 Yalaxiang trench

The Selaha fault along the northern Kangding faults is a sequence of moraine ridges, fluvioglacial accumulation platforms, and fluvioglacial terraces, yielding structural landforms such as linear troughs and fault ponds. On the south side of Chongcaoping, we excavated a trench in the fault trough, which spanned the entire fault depression. This trench's north wall collapsed during excavation, while the south wall was in good

10.3389/feart.2023.1140326

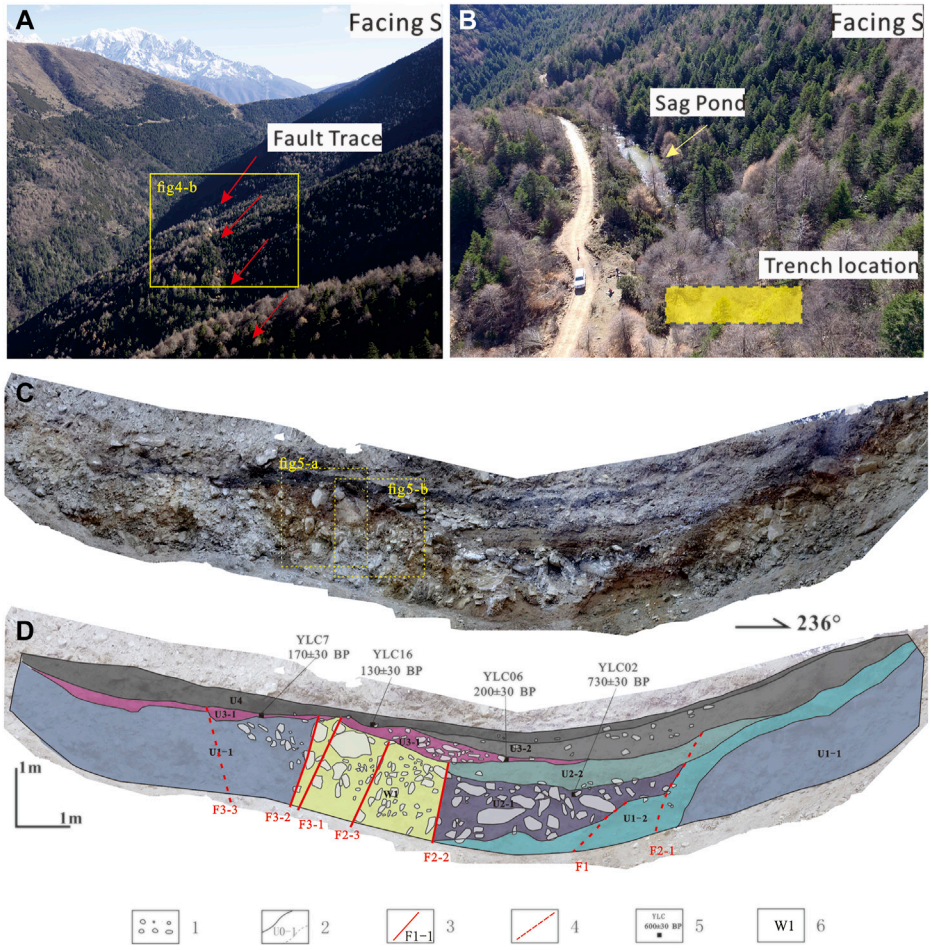

FIGURE 4
Fault traces and locations of trenches. Faulted landforms near Yalaxiang township **(A,B)**. **(C)** photographic mosaic of the south wall of the trench; **(D)** interpretation log(lower) of the trench. 1) Gravel; 2) depositional unit sequence and stratigraphic boundary (dotted line indicates the unclear boundary); 3) fault trace; 4) speculate fault; 5) location and dating of ^{14}C samples; and 6) structural wedge.

TABLE 2 Units and descriptions exposed by the Yalaxiang trench.

Unit	Description
U1	Clay-containing gravel layer, containing boulder can be divided into two sublayers according to the content of clay. U1a is an earthy yellow gravel layer, semiconsolidated, and formed by the accumulation of alluvial facies; U1-b is a dark-yellow clay layer with gravel and slope accumulation
U2	Fault pond sedimentation, both sides controlled by faults, the strata appear bowl-shaped, can be divided into two sublayers. U2a is a black organic soil layer, and the AMS dating result of a carbon chip at the top is 730 ± 30 BP. U2b is a fine gray–yellow sand layer with horizontal layers
U3	The clay layer, which can be divided into two sublayers. U3a is a black organic soil layer with a thin layer; AMS dating results were 200 ± 30 BP and 170 ± 30 BP, respectively; U3b is a gray gravel-bearing clay layer
U4	The light-yellow clay layer can be divided into three sublayers according to color and sedimentary characteristics, U4a is an earthy yellow gravel-bearing fast clay layer, and the carbon-like AMS dating result is 880 ± 20 BP. U4b is a light earthy yellow clay layer, and the carbon-like AMS dating result is 495 ± 25 BP. U4c is an earthy yellow clay layer, and the carbon AMS dating result is 360 ± 40 BP.
U5	The black clay layer, which contains a large amount of organic matter in the middle of the trough, and the MS dating result of 1carbon chip at the bottom is 130 ± 30 BP.

shape (Figure 4). The trench profile reveals that there are multistage fault pond sediments and alluvial–pluvial deposits on the eastern side, while the alluvial deposits along the slope dominate the western side. According to the sedimentary characteristics, it can be roughly divided into four sets of strata, including six sublayers (Table 2).

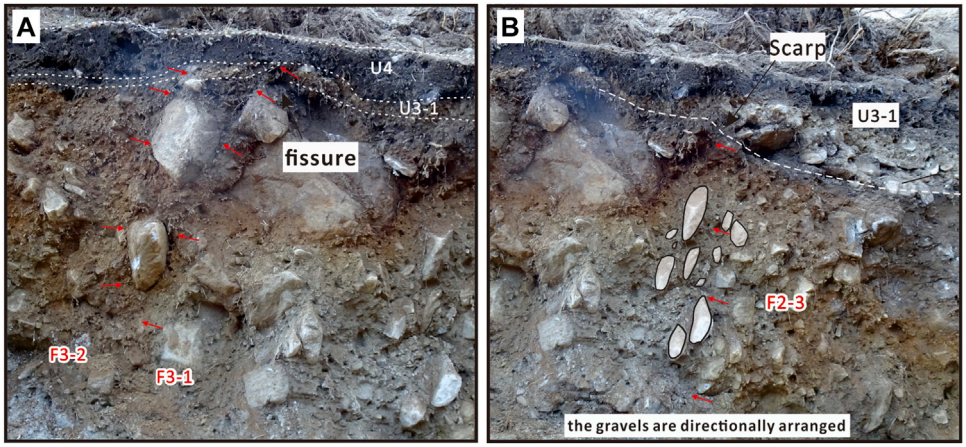

FIGURE 5
Close shots of the local topical partial trench wall and the details of the fault. **(A)** the fault trace of F3-2/F3-1. **(B)** the fault trace of F2-3.

Two palaeoseismic events, SL1 and SL2, can be identified by stratigraphic evidence according to the relationship between faulting and sedimentation in the sedimentary sequences of the fault depression, and the times of the two events were restricted to between U2-2 and U3-1 and U3-2 and U4-l, respectively.

The main evidence of event SL1 is as follows: ①the stratigraphic boundary is very clear: layer U2-2 is fine sand, while the bottom of U3 is an organic clay layer with gravel, which means that the sedimentary facies of the strata has changed; ② the topographic uplift on the eastern side of the trench is caused by fault F2-1/F2-2/F2-3, which faults layer U2-2. Layer U3-1 is a local gravel layer that formed quickly in front of the ridge (Figure 5B).

The main evidence for SL2 is as follows: ①clear stratigraphic and sedimentary boundaries; ②layer U3-1 is deformed and faulted along faults F3-2 and F3-1, and it is arched and faulted along fault F3-3 (Figure 5A), whereas layer U4 above it covers it firmly and without any deformation.

Four carbon debris samples were obtained and sent to Beta Laboratory for accelerated mass spectrometry (AMS) dating. At a 95.4% confidence interval (Table 4), the calendar ages of the two events from OxCal 4.4 are as follows: SL1, 1272–1720 AD; SL2, 1703–1929 AD.

4.3 Zheduotang trench

The Zheduotang fault delineates a string of ridges from Zheduoshan to Zheduotang village, creating fault ponds, fault troughs, and slope ridges. The surface rupture of the 1955 M $7^1/_2$ earthquake formed a 1.8 m reverse scarp on alluvial–diluvial terrace

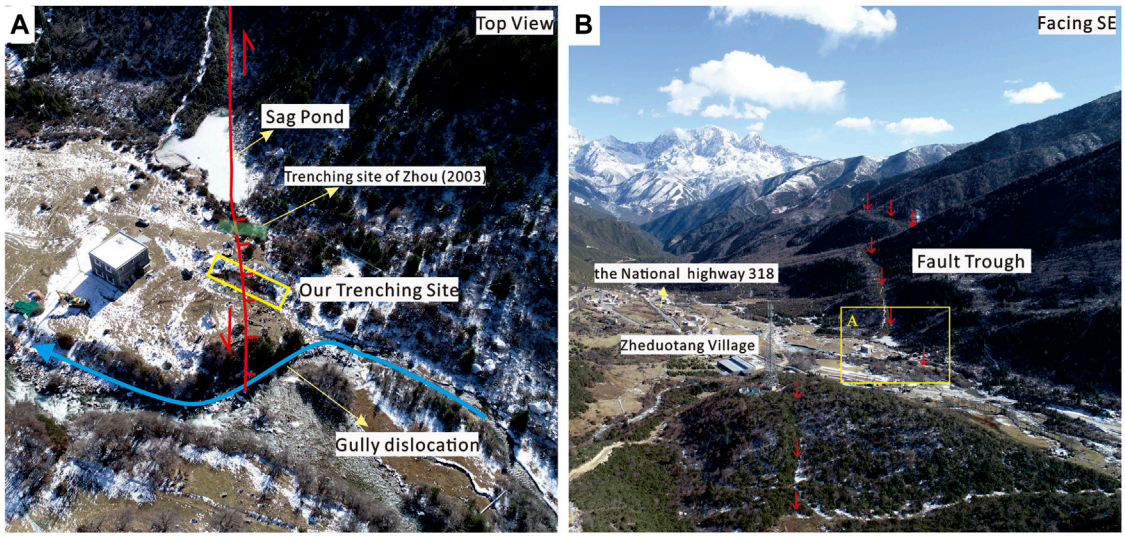

FIGURE 6
Fault field photographs of the fault traces near the Zheduotang Village. **(A)** Representative faulted landforms. **(B)** The location of Zheduotang trench.

10.3389/feart.2023.1140326

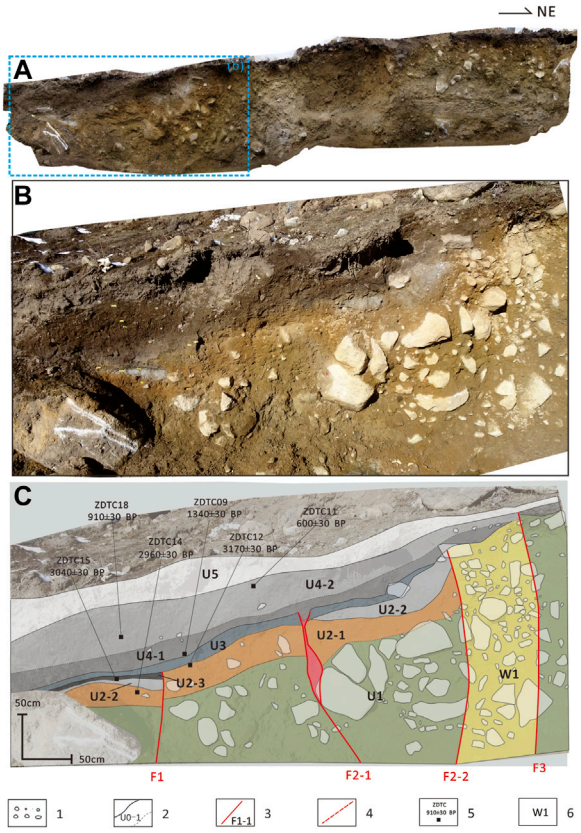

FIGURE 7
Photographic mosaic **(A–B)** and interpretation log **(C)** of the Zheduotang trench. a, photographic mosaic of the north wall of the trench; b, close shots of the local topical partial trench wall; and c, interpretation log(lower) of the trench. 1) Gravel; 2) depositional unit sequence and stratigraphic boundary (dotted line indicates the unclear boundary); 3) fault trace; 4) speculate fault; 5) location and dating of ^{14}C samples; and 6) structural wedge.

T1 along the fault, which is distributed on the right step near Zheduotang village. The Zheduotang trench crosses the fault scarp (Figure 6). On the western side of the trench, there is a sandy gravel layer of terrace alluvium and diluvium with a lenticular sand layer, while on the eastern side, there are deposits from many stages of fault depression (Figure 7). Because of gurgling and flooding in the low-lying section of the western wall, only a portion of the walls was kept. According to the sedimentary characteristics, the site can be divided into five sets of strata, including three sublayers. The strata are shown in Table 3.

There was a fault zone with a width of approximately 1 m that ruptured upward to the ground surface (Figures 7A, B), which should correspond to the 1955 *M* 7 earthquake. The strata in the sag-pond have experienced faulting, fold deformation, and fracture filling to varying degrees since the fault zone governs these processes. Based on this deformation evidence and depositional sequences, three events can be identified.

Event ZD1 occurred after U2-3 and before U3. The main evidence is as follows: ①the boundary of strata deposition is very clear; U2-3 is an organic layer rich in carbon debris, and there is a sedimentary phase change with U3, which does not include carbon debris; ②F1 faults layer U2 and is covered by layers U3.

Event ZD2 occurred after U3 and before U4-1. The main evidence is as follows: ①F2-1 faults U3, dragging it into the structural zone, and U4-1 fills the gap along the fracture (Figure 7C); ②along fault F2-2, which causes U2 and U3 bending deformation, the gravels are directionally arranged, and U4 covers it (Figure 7C).

Event ZD3 occurred after U4-2 and before U5. The gravels in F3 are directionally organized to the surface, with clear fault traces. A scarp can be observed on the surface, which should be associated with the 1955 AD earthquake.

Six carbon debris samples were obtained and sent to Beta Laboratory for accelerated mass spectrometry (AMS) dating. At a 95.4% confidence interval (Table 4), the calendar ages of the two events from OxCal 4.4 are as follows: ZD1, 1215 BC ~ 315 AD; ZD2, 830 BC ~ 705 AD. The latest event, ZD3, is after 1500 AD.

4.4 Lianhecun trench

From the Zhuma basin to the Huilong uplift, several faulted landforms, including the fault trough, water system, ridge

TABLE 3 Units and descriptions exposed by the Zheduotang trench.

Unit	Description
U1	The light-green pebbly clay is formed by piedmont alluvial–pluvial facies. It can be divided into three sublayers from top to bottom. The top is brown–yellow clay (U2a), containing a small amount of gravel; middle U2b grayish white mud layer, controlled by fault; The top is U2c black organic clay layer, in which a carbon fragment is collected, and the AMS dating result is 3010 ± 30 BP
U2	The light-green pebbly clay is formed by piedmont alluvial–pluvial facies. It can be divided into three sublayers from top to bottom. The top is brown–yellow clay (U2a), containing a small amount of gravel; middle U2b grayish white mud layer, controlled by fault; The top is U2c black organic clay layer, in which a carbon fragment is collected, and the AMS dating result is 3010 ± 30 BP
U3	A grayish green clay layer, with a clear boundary line with the underlying strata, accumulated along the ridge, a stable layer thickness of grayish black clay layer, mixed with small gravel blocks, which can be divided into two sublayers U4a and U4b according to the content of organic matter. AMS dating result of a carbon fragment at the bottom is 1340 ± 30 BP; U4b is a grayish black clay layer, containing a large amount of organic matter. Two carbon fragments were collected from this layer, and the AMS dating results are 600 ± 30 BP and 910 ± 30 BP, respectively. Now, it represents the development of soil layers and grass roots
U4	A grayish green clay layer, with a clear boundary line with the underlying strata, accumulated along the ridge, a stable layer thickness of grayish black clay layer, mixed with small gravel blocks, which can be divided into two sublayers U4a and U4b according to the content of organic matter. AMS dating result of a carbon fragment at the bottom is 1340 ± 30 BP; U4b is a grayish black clay layer, containing a large amount of organic matter. Two carbon fragments were collected from this layer, and the AMS dating results are 600 ± 30 BP and 910 ± 30 BP, respectively
U5	Surface layer; the development of soil layers and grass roots

TABLE 4 Radiocarbon samples and dating results for the four trenches.

Sample	Lab code	$^{13}C/^{12}C$ (o/oo)	Radiocarbon age (years BP±σ)	Calendar years (cal BP)	Description	Unit sampled
				2σ(95.4%)		
ZDTC11	548371	-25.1	600 ± 30	1295-1410AD	Charcoal	ZD/U4-2
ZDTC18	548375	-22.9	910 ± 30	1030-1205AD	Charcoal	ZD/U4-2
ZDTC09	548370	-24.0	1340 ± 30	640-715AD (83.4%)	Charcoal	ZD/U4-1
				740-770AD (12.0%)		
ZDTC15	548374	-23.2	3040 ± 30	1400-1215BC	Charcoal	ZD/U2-3
ZDTC14	548373	-22.9	2960 ± 30	1265-1055BC	Organic sediment	ZD/U2-1
ZDTC12	548372	-22.9	3170 ± 30	1505-1395BC	Charcoal	ZD/U2-1
YLC16	548379	-24.4	130 ± 30	1804-1950AD	Charcoal	SL/U4
YLC07	548378	-23.6	190 ± 30	1655-1705AD (36.7%)	Charcoal	SL/U3-1
				1719-1816AD (58.7%)		
YLC06	548377	-24.7	200 ± 30	1648-1687AD (36.7%)	Charcoal	SL/U3-1
				1732-1806AD (58.7%)		
YLC02	548376	-26.8	730 ± 30	1225-1234AD (1.7%)	Charcoal	SL/U2-3
				1240-1299AD (92.1%)		
				1371-1379AD (1.6%)		
A2	--	-21.8	495 ± 25	1407-1446 AD	Charcoal	BCS/U4b
A3	--	-22.9	360 ± 40	1450-1634 AD	Charcoal	BCS/U4c
A4	--	-23.2	880 ± 20	1055-1219 AD	Charcoal	BCS/U4a
A7	--	-24.3	1045 ± 5	988-1019 AD	Charcoal	BCS/U3
C7#	--	--	1700 ± 100	--	Charcoal	BCS*/U3
LH-C39	514443	-28.5	250 ± 30	1521-1578AD (22.5%)	Charcoal	LH/U5
				1625-1677AD (72.9%)		
LH-C40	52559	-24.6	230± 30	1524-1559AD (6.9%)	Charcoal	LH/U5
				1631-1685AD (88.2%)		
				1786-1790AD (0.3%)		
LH-C73	521562	-26.2	170 ± 30	1667-1689AD (7.3%)	Charcoal	LH/U6
				1721-1823AD (73.3%)		
				1831-1880AD (10.2%)		
				1917-1944AD (4.8%)		
LH-C61	521564	-24.4	390 ± 30	1441-1524AD (69.2%)	Charcoal	LH/U5
				1570-1630AD (26.2%)		
LH-C102	514433	-25.8	390 ± 30	1441-1524AD (69.2%)	Charcoal	LH/U5
				1570-1630AD (26.2%)		
LH-C109	521563	-24.8	170± 30	1667-1698AD (7.1%)	Charcoal	LH/U6
				1721-1823AD (73.2%)		
				1831-1880AD (10.2%)		
				1917-1944AD (4.9%)		

(Continued on following page)

TABLE 4 (*Continued*) **Radiocarbon samples and dating results for the four trenches.**

Sample	Lab code	$^{13}C/^{12}C$ (o/oo)	Radiocarbon age (years BP±$^{\sigma}$)	Calendar years (cal BP)	Description	Unit sampled
				2σ(95.4%)		
LH-C104	514434	-26.4	140 ± 30	1677-1783AD (47.2%)	Charcoal	LH/U6
				1796-1891AD (43.9%)		
				1913-1934AD (4.3%)		

*BCS: Baichunshu trench; SL: Yalaxiang trench; ZD: Zheduotang trench; LH: Lianhecun trench; #C7 are the results of conventional^{14}C dating (tested by the Institute of Geology, China Earthquake Administration).

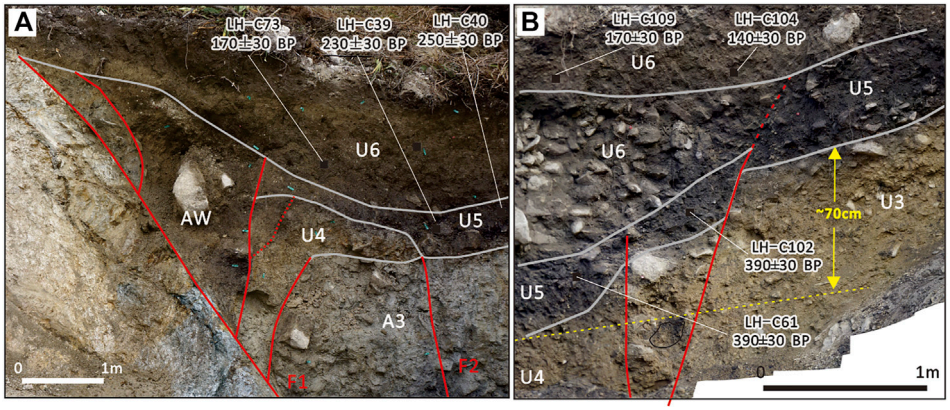

FIGURE 8
Close shots of the local topical partial trench wall and the details of the latest event in the Lianhecun trench. **(A)** Details of the south wall of Lianhecun TC1 (Feng et al., 2021); **(B)** details of the north wall of Lianhecun TC2; 70 cm indicates an apparent vertical dislocation.

dislocation, and minor fault depression, were formed along the Shimian fault. The fault trough and tiny fault depression are very visible at Lianhecun, where the left-lateral dislocation of the gully is approximately 107 m. Two trenches (Feng et al., 2021) were excavated across one of the small fault ponds. Four events were revealed: E1, 20925–116850 BC; E2, 15265 BC ~ 1785 BC; E3, 360 AD ~ 1475 AD; and E4, 1655 AD ~ 1815 AD.

The latest event that the trench showed is quite obvious. Between U5 and the primary fault zone F1 on the southern wall (Figure 8A), there is wedge-shaped filling (AW). The black soil in layer U5 was filled into the AW, and overlying layer U6 had not deformed. On the northern wall, there was a bottom gravel layer in U6 (Figure 8B), which indicates a change in the sedimentary environment. There were approximately 70 cm vertical dislocations along the fault. Seven samples of carbon debris from U4 and U5 were sent to the Beta Laboratory in the United States for AMS dating. The initial date was adjusted using the age correction program OxCal4.44 (Table 4), and the event occurred between 1655 and 1815 AD.

5 Discussion

As a result, the latest event of the northern segment of the Anninghe fault revealed by the Baichunshu trench occurred after 1535 AD The latest two events, SL1: 1272–1720 AD and SL2: 1703–1929 AD, in the Selaha fault were revealed by the Yalaxiang trench. The latest event of the Zheduotang fault occurred after 1500 AD by the Zheduotang trench. The latest event of the Shimian fault was exposed by the Lianhecun trench between 1655 and 1815 AD. Additionally, the Xingyulin trench found that the Moxi fault's most recent event occurred between 1280 and 1850 AD (Gao et al., 2021), while the Yalahe fault's most recent event may have been the 1700 AD earthquake (Liang et al., 2020) (Figure 9).

Since 1700 AD, four earthquakes of $M \geq 6.5$ have been recorded in the history of the area from Kangding to Shimian in the order of the 1725 AD M 7 Kangding earthquake, the 1748 AD M $6^1/_2$ earthquake in northwest Kangding, the 1786 AD M $7^3/_4$ earthquake in southern Kangding, and the 1955 AD M $7^1/_2$ Kangding earthquake (Department of Earthquake Disaster Prevention, 1995). Among them, the elapsed time of the 1955 AD M $7^1/_2$ Kangding earthquake is the shortest. This earthquake left a surface rupture zone of about 30 km along the Zheduotang fault (The Chengdu Seismic Brigade, 1972). According to prior knowledge and earthquake cases, an earthquake's magnitude that results in a surface rupture on the Chinese mainland is often greater than M $6^3/_4$ (Deng et al., 1992). There were only few kilometers of ambiguous surface rupture from the Luding M 6.8 earthquake in 2022 AD (Li et al., 2022; Han et al., 2023). It is concluded that the 1748 AD Kangding M $6^1/_2$ earthquake may not have

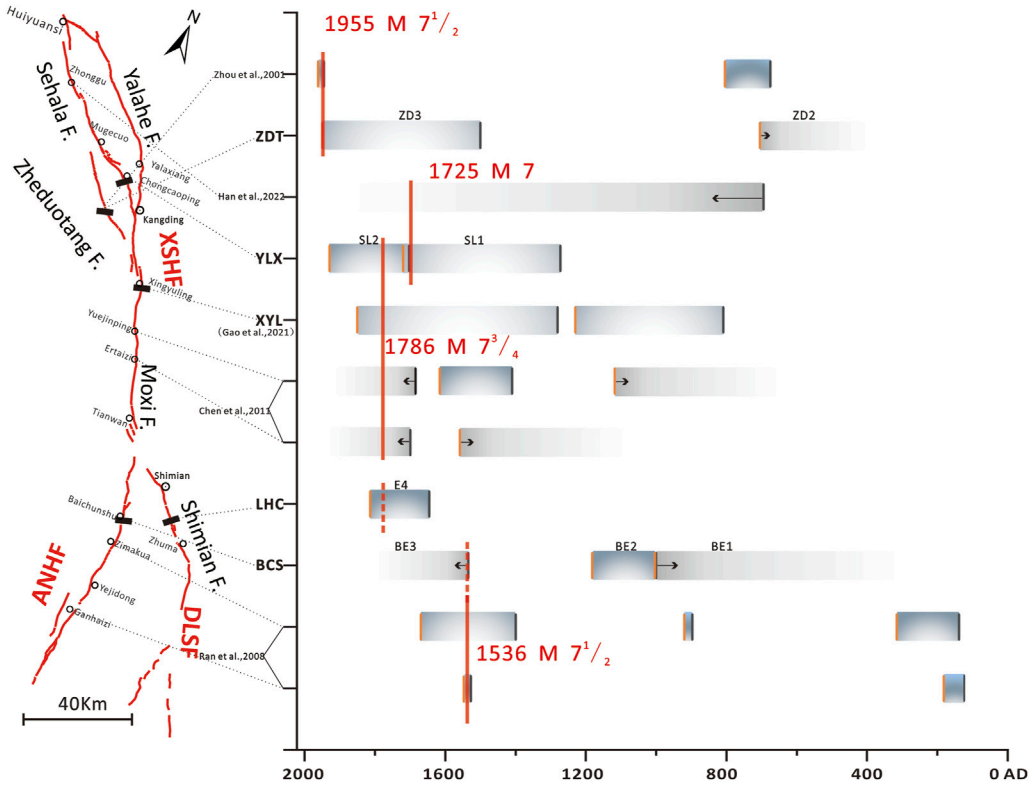

FIGURE 9
Palaeoseismic sequence from trenching at different sites and compared with historical record earthquakes. The gradient area represents the range of palaeoseismic events revealed by different trenches. The orange vertical line is the upper limit of the event, while the black vertical line is the lower limit of the event.

produced a surface rupture. A 100 m-long ground fissure was discovered on the moraine gravel platform at Chongcaoping, the epicenter of the AD 1725 Kangding *M* 7 earthquake, and the gravel there exhibited clear twisting marks (Wang, 1992; Li, 1997). It is possible that event SL1 revealed by the Yalaxiang trench, which was excavated 500 m south of Chongcaoping in the meizoseismal region of the 1725 earthquake, was the earthquake. However, the meizoseismal region of the 1786 AD earthquake extends from Kangding to Shimian (Department of Earthquake Disaster Prevention, 1995). The prior study results and the Xingyulin trench indicate that a surface rupture occurred during the earthquake in the Kangding–Moxi region (Gao et al., 2021). Some investigations have suggested that the northwest end may extend to the vicinity of Mugecuo, and the southeast end may reach the Tianwan area (Wang and Pei, 1998; Zhou et al., 2001b). Yalaxiang trench data show that the most recent incident SL2 closely matches the 1786 earthquake. According to the degree of bending deformation and elevation in the trench profile, the trench site should be located near the northernmost end of the surface rupture. In recent years, some new evidence has been obtained in the southeastward of the rupture, which shows that the rupture extends at least to the south of Tianwan (Chen et al., 2011, 2016). The results from the Lianhecun trench indicate that the most recent event in the Shimian fault occurred between 1655 and 1815 AD. Since 1500 AD, the historical earthquake data of $M \geq 7$ in this area have been complete (Huang and Li, 1994). Except for the 1786 Kangding earthquake, no unambiguous written records of earthquakes have been discovered in Shimian since the Ming and Qing Dynasties, according to historical earthquake records (Gu, 1983; Department of Earthquake Disaster Prevention, 1995; Sun, 2010). So, the 1786 earthquake should be considered the most recent seismic event on the Shimian fault, which is constrained by the Lianhecun trench.

By excavating the trench groups in Zimakua, Ganhaizi, and Dahaizi, Ran et al. (2008) proposed that the northern segment of the ANHF can be separated into two distinct subsections, namely, the Dahaizi–Ganhaizi section and the Zimakao–Yejidong section. In the northern part of the Zimakao–Yejidong section, three palaeoseismic events occurred: 280–550 B.P., 1030–1050 B.P., and 1634–1811 B.P. The three events disclosed by the Baichunshu trench correspond to the most recent three occurrences at the site of the Zimakua trench (Figure 9). Wang et al. (2014) examined palaeoseismic data from the southern and northern parts of the ANHF and determined that the 1536 Xichang M $7^1/_2$ earthquake ruptured the whole length. The latest event (after 1535 AD) revealed by the Baichunshu trench may correspond to the 1536 Xichang M $7^1/_2$ earthquake. However, due to the lack of historical records, it cannot be completely ruled out that the latest event revealed by the Baichunshu trench may also be the 1786 earthquake (Figure 9).

In summary, the latest event limited by the Baicunshu and Zheduotang trenches cannot rule out the 1786 AD earthquake. This earthquake ruptured the Shimian fault (the northern section of the DLSF) and the southern segment of the XSHF, with a total length of approximately 120 km from the northern end near the Yalaxiang trench to the southern end on the south side of the Lianhecun trench. Similar to

the *Ms* 8.0 2008 Wenchuan earthquake and the *Mw* 7.8 2016 Kaikōura earthquake (Tan et al., 2013; Hamling et al., 2017), this earthquake is also a complex earthquake with a multi-fault rupture.

According to the empirical relationship between the length of the surface rupture of the strike-slip fault type and the magnitude of earthquake occurrence,

$$M = 5.16(\pm 0.13) + 1.12(\pm 0.08)*\log(SRL),$$

where *M* is the magnitude of the earthquake, SRL is the surface rupture length, and the values in brackets are the error coefficients (Wells and Coppersmith, 1994). If the length is 120 km, the magnitude of the earthquake is approximately *M* $7^3/_4$, which is equivalent to the estimated result of historical earthquake intensity.

Furthermore, according to historical records, there was an aftershock of magnitude 6 or greater on June 2 after the major earthquake of magnitude *M* $7^3/_4$ on 1 June 1786 AD, and there may have been an earthquake of magnitude 7 or greater near Detuo on June 10 (Sun, 2010). It also reflects that the 1786 AD *M* $7^3/_4$ earthquake along the XSHF may have triggered the rupture of the Shimian fault, resulting in multi-fault rupture behavior.

6 Conclusion

Four trenches, excavated in the vicinity of the epicenter in the northern section of DLSF, the northern section of the ANHF, the Zheduotang fault, and the Salaha fault of the XSHF, revealed the depositional sequences and deformation evidence in the palaeoearthquakes. The major results are given as follows:

1) From trenching and ^{14}C ages, two palaeoseismic events have occurred on the northern section of the ANHF: BE1, ~1003AD; BE2, 1000–1182AD. We associate the most recent event BE3 with the historical records of 1536 AD *M* 7.
2) Two palaeoseismic events have occurred on the Selaha fault in the last 500 years, SL1, 1272–1720 AD; SL2, 1703–1929 AD. We associate two young events with the historical records of the 1725 AD Kangding *M* 7 earthquake and the 1786 AD Kangding *M* $7^3/_4$ earthquake.
3) Three palaeoseismic events have occurred on the Zheduotang: ZD1, 1215 BC ~ 315 AD; ZD2, 830 BC ~ 705 AD; and ZD3, 1955 AD Kangding *M* $7^1/_2$ earthquake.
4) The 1786 AD Kangding *M* $7^3/_4$ earthquake was probably a multi-fault event, based on the trenching profile evidence, the nearby offset geomorphic features, and the historical earthquake data. This earthquake's seismogenic fault is the Moxi fault, which triggered the southern end of the Selaha fault to the north and the Shimian fault (DLSF) to the south. The total rupture length is approximately 120 km.

Data availability statement

The original contributions presented in the study are included in the article/Supplementary Material; further inquiries can be directed to the corresponding author.

Author contributions

The study was designed by LC; the field work was carried out by MH, YL, SG, JF, LL, and LC; the writing and preparation of the original manuscript were carried out by JF; and the review and editing of the final manuscript were performed by LC, MH, and CS. All authors contributed to the article and approved the submitted version.

Funding

This work was supported financially by the National Natural Science Foundation of China (41872228, 41672207), the Second Tibetan Plateau Scientific Expedition and Research (2019QZKK0901), and the Basic Scientific Work of the Institute of Geology, China Earthquake Administration (IGCEA1418).

Acknowledgments

The authors thank Prof Ran Yongkang for meticulous guidance on the exploration and thesis research work. They also would like to thank Deng Jinhua for the careful revision of the paper format. The authors give great thanks to Wenjun Zheng, Chuanyong Wu, Daoyang Yuan and Jun Shen for their constructive suggestions to improve the article.

Conflict of interest

The authors declare that the research was conducted in the absence of any commercial or financial relationships that could be construed as a potential conflict of interest.

Publisher's note

References

Allen, C. R., Luo, Z. L., Qian, H., Wen, X. Z., Zhou, H. W., and Huang, W. S. (1991). Field study of a highly active fault zone: The Xianshuihe fault of southwestern China. *Geol. Soc. Am. Bull.* 103, 1178–1199. doi:10.1130/0016-7606(1991)103<1178:fsoaha>2.3.co;2

An, Y. F. (2010). *Study on the boundary characteristics of seismic rupture segments in Xianshuihe fault zone*. Ph.D. Thesis. China Earthquake Administration: Institute of Geology. (in Chinese with English Abstract).

Ch, G., Papadimitriou, E. E., Karakostas, V. G., Wen, X. Z., Jin, X. S., Kilas, A., et al. (2008). Implication of fault interaction to seismic hazard assessment in Sichuan-Yunnan provinces of southeastern China. *Earthq. Sci.* 21, 181–201. doi:10.1007/s11589-008-0009-7

Chen, G. H., Xu, X. W., Wen, X. Z., and Chen, Y. G. (2016). Late quaternary slip-rates and slip partitioning on the southeastern Xianshuihe fault system, eastern Tibetan plateau. *Acta Geol. sin.* 90, 537–554. doi:10.1111/1755-6724.12689

Chen, G. Y., Min, W., and Song, F. M. (2011). Preservation of co-seismic surface rupture in diffrrent geomorphological settings from the study of the 1786 Moxi earthquake (in Chinese with English Abstract). *Seismol. Geol.* 33 (4), 804–817.

Chen, G. Y. (2006). *Tectonic transformation and deformation demarcation of the active tectonic belt on the northeast boundary of the Sichuan-Yunnan block (in Chinese)*. Ph.D. Thesis. China Earthquake Administration: Institute of Geology.

Chen, L. C., Li, Y. B., and Gao, S. P. (2018). Fracture behavior of multiple faults and prediction of large earthquakes (in Chinese). 24: 24–24

China News Network (2022). *Sichuan Luding earthquake has caused 93 deaths and 25 missing*. Available at: https://www.chinanews.com.cn/sh/2022/09-12/9850488.shtml.

The Chengdu Seismic Brigade (1972). *A suggestion on that medium and long term earthquake prediction in Shimian-Kangding area (in Chinese)*.

Deng, Q. D., Yu, G. H., and Ye, W. H. (1992). *Study on relationship between earthquake surface rupture and earthquake magnitude (in Chinese)*. Beijing: Study on Active Faults, 247–264.

Deng, Q. D., Zhang, P. Z., Rang, Y. K., Yang, X. P., Min, W., and Chun, Q. Z. (2002). Basic characteristic of active tectonics in China (in Chinese with English Abstract)(. *Sci. Chinaseries D)* 32 (12), 1020–1030.

Department of Earthquake Disaster Prevention (1995). "State seismological bureau," in *Catalogue of historical strong earthquakes in China (23rd century B.C.to 1911)* (Beijing: Seismological Press), 1–514. (in Chinese).

Department of Earthquake Disaster Prevention (1999). "State seismological bureau," in *Catalogue of modern earthquakes in China (1912-1990)* (Beijing: Seismological Press), 1–637. (in Chinese).

Feng, J. H., Chen, L. C., Wang, H., Li, J., Han, M. M., Li, Y. B., et al. (2021). Paleoseismologic study on the Shimian fault in the northern section of daliangshan fault zone (in Chinese with English Abstract). *Seismol. Geol.* 43 (1), 53–71.

Fletcher, J. M., Teran, O. J., Rockwell, T. K., Oskin, M. E., Hudnut, K. W., Mueller, K. J., et al. (2014). Assembly of a large earthquake from a complex fault system: Surface rupture kinematics of the 4 april 2010 el mayor-cucapah (Mexico) *Mw* 7.2 earthquake geosphere. *Geosph. (Boulder).* 10, 797–827. doi:10.1130/ges00933.1

Gan, W. J., Zhang, P. Z., Shen, Z. K., Niu, Z. J., Wang, M., Wan, Y. G., et al. (2007). Present-day crustal motion within the Tibetan Plateau inferred from GPS measurements. *J. Geophys. Res. Solid Earth* 112 (B8), B08416. doi:10.1029/2005JB004120

Gao, W., He, H, L., Sun, H. Y., and Wei, Z. Y. (2016). Paleoearthquakes along puxiong fault of daliangshan fault of daliangshan fault zong in Chinese with English Abstract. *Seismol. Geol.* 38 (4), 797–816.

Gao, S. P., Chen, L. C., Liang, M. J., Wang, D., Li, Y. B., Han, M. M., et al. (2021). Rupture characteristics and seismic recurrence behaviors of Xianshuihe fault reveals by Xingyulin trences, south of kangding (in Chinese with English abstract). *Adv. Eng. Sci.* 53 (3), 53–61.

Gu, G. X. (1983). *The Catalogue of Chinese earthquake (from 1831 B.C. to 1969 A.D)*. Beijing: China Science and Technology Press, 1–300. (in Chinese).

Han, B. Q., Liu, Z. J., Chen, B., Li, Z. H., Yu, S., Zhang, Y., et al. (2023). Coseismic deformation and slip distribution of the 2022 luding Mw 6.6 earthquake revealed by InSAR observations. *Geomatics Inf. Sci. Wuhan Univ.* 48 (1), 36–46. doi:10.13203/j.whugis20220636

Hamling, I. J., Hreinsdóttir, S., Clark, K., Eliott, J., Liang, C., Fielding, E., et al. (2017). Complex multifault rupture during the 2016 M_w 7.8 Kaikōura earthquake, New Zealand. *Science* 356, eaam7194. doi:10.1126/science.aam7194

Han, M. M., Chen, L. C., Zeng, D., Li, Y. B., Liang, M. J., Gao, S. P., et al. (2022). Discussion on the latest surface ruptures near the Zhonggu village along the Selaha segmentof the Xianshuihe fault zone (in Chinese). *J. Geomechanics* 28 (6), 969–980. doi:10.12090/j.issn.1006-6616.20222824

He, H. L., Ikeda, Y., He, Y. L., Chen, J., Chen, C. Y., et al. (2008). Newly-generated Daliangshan fault zone-ShortCutting on the central section of xianshuihe-xiaojiang fault system. *Sci. China Ser. D Earth Sci.* 51 (9), 1248–1258. doi:10.1007/s11430-008-0094-4

Huang, W. Q., and Li, W. X. (1994). Study on completeness of seismic data in China's continent (2): The beginning year of basically complete seismic data in different regions. *Earthquake* 16 (4), 10 [in Chinese].

Institute of Geology, CEA (2019). *Map of the northern section of the Anning River active fault*, 1. Beijing: Seismological Press, 50000. (in Chinese).

Li, T. T. (1997). *The Xianshuihe fault zone and assessment of strong earthquake risk (in Chinese)*. Chengdu: Science and Technology Press of Sichuan, 1–315.

Li, Y., Zhao, D., Shan, X., Gao, Z., Huang, X., and Gong, W. (2022). Coseismic slip model of the 2022 Mw 6.7 Luding (Tibet) earthquake: Pre- and post-earthquake interactions with surrounding major faults. *Geophys. Res. Lett.* 49, e2022GL102043. doi:10.1029/2022GL102043

Liang, M. J., Chen, L. C., Ran, Y. K., Li, Y. B., Wan, D., Gao, S. P., et al. (2020). Late-quaternary activity of the Yalahe fault of the Xianshuihe fault zone, eastern maprgin of the Tibet plateau (in Chinese with English Abstract). *Seismol. Geol.* 42 (2), 514–525.

Long, D. X., and Deng, T. G. (1986). A preliminary study on segment feature of fault motion along Xianshuihe fault belt ((in Chinese with English Abstract)). *J. deismological Res.* 5 (9).

Lozos, J. C., Oglesby, D. D., Duan, B., and Wesnousky, S. G. (2017). The effects of double fault bends on rupture propagation: A geometrical parameter study. *Bull. Seismol. Soc. Am.* 101, 385–398. doi:10.1785/0120100029

Ma, J., Zhou, B. G., Wang, M. M., and An, L. K. (2022). Geological and geomorphic evidences for the Holocene activity of the NW zheduotang brance within the Xianshuihe fault system ((in Chinese with English Abstract)). *Seismol. Geol.* 42 (05), 1021–1038.

Mark, S. B., Nicola, L., Pilar, V., Andy, N., Jarg, P., Phillip, B. S., et al. (2017). The Mw7.8 2016 Kaikōura earthquake: Surface fault rupture and seismic hazard context. *Bull. N. Z. Soc. Earthq. Eng.* 50 (2), 73–83.

Onderdonk, S., McGill, S., and Rockwell, T. (2018). A 3700 yr paleoseismic record from the northern San Jacinto fault and implications for joint rupture of the San Jacinto and San Andreas faults. *Geosphere* 14 (6), 2447–2468. doi:10.1130/ges01687.1

Qian, H., Allen, C. R., Luo, Z. L., Wen, X. Z., Hou, H. W., and Huang, W. S. (1988). The active characteristics of Xianshuihe fault in Holocene ((in Chinese with English Abstract)). *Sci. China* 02, 11–20.

Ran, Y. K., Chen, L. C., Cheng, J. W., and Gong, H. L. (2008a). Late Quaternary surface deformation and rupture behavior of strong earthquake on the segment north of Mianning of the Anninghe Fault. *Sci. China (Ser D)* 51 (9), 1224–1237. doi:10.1007/s11430-008-0104-6

Ran, Y. K., Chen, J. W., Gong, H. L., and Chen, L. C. (2008b). Late Quaternary geomorphic deformation and displacement rates of the aninghe fault around zimakua (in Chinese with English Abstract). *Seismol. Geol.* 30 (1), 86–98.

Ran, Y. K., Wang, H., Li, Y. B., and Chen, L. C. (2012a). Key techiques and several cases analyisis in paleoseismic studies in mainland China (1): Trenching sites, layouts and paleoseismic indicators on active strike-slip faults (in Chinese with English abstract). *Seismol. Geol.* 34 (2), 14.

Ran, Y. K., Wang, H., Li, Y., and Chen, L. C. B. (2012b). Key techiques and several cases analyisis in paleoseismic studies in mainland China (5): nonvisibility,dieout of fault strands and identification of young paleoseismic events(in Chinese with English abstract). *Seismol. Geol.* 34 (2), 197–210.

Ramsey, C. B. (2009). Bayesian analysis of radiocarbon dates. *Radiocarbon* 51 (1), 337–360. doi:10.1017/s0033822200033865

Reimer, P. J., Bard, E., Bayliss, A., Beck, J. W., Blackwell, P. G., Ramsey, C. B., et al. (2013). IntCal13 and Marine13 radiocarbon age calibration curves 0-50,000 years cal BP. *Radiocarbon* 55 (4), 1869–1887. doi:10.2458/azu_js_rc.55.16947

Scharer, K., Ray, W., Glenn, B., Ashley, A., and Thomsa, F. (2017). Ground-rupturing earthquakes on the northern big bend of the san andreas fault California, 800 A.D. To present. *J. Geophys. Res. Solid Earth* 122, 2193–2218. doi:10.1002/2016jb013606

Stirlinghv, M. W., Litchfield, N., Villamor, P., Dissen, R., Nicol, A., Pettinga, J., et al. (2017). "The Mw7.8 2016 Kaikōura earthquake: Surface fault rupture and seismic hazard context," in *Bulletin of the New Zealand Society for Earthquake Engineering* 50, 73–84.

Sun, C. M. (2010). *A compilation of sichuan historical earthquakes editorial board (from 26 B.C. To 1949.9 A.D.)*. Chengdu: Sichuan People's Publitshing house, 13–15. (in Chinese).

Sun, H. Y., He, H. L., and Wei, Z. Y. (2015). Late quaternary activity of zhunma fault on the north segment of daliangshan fault zone (in Chinese with English Abstract). *Seismol. Geol.* 37 (2), 440–454.

Sun, H. Y., HeIkedaWei, H. L. Y. Z. Y., Chen, Y. R., Shi, F., Chen, C., Xu, Y., et al. (2019). Paleoearthquake history along the southern segment of the Daliangshan fault zone in the southeastern Tibetan Plateau. *Tectonics* 38 (4), 2208–2231. doi:10.1029/2018TC005009

Tan, X. B., Yuan, R. M., Xu, X. W., Chen, G. H., and Chang, C. P. (2013). Co-seismic rupture and displacement in the Xiaoyudong area produced by the 2008 Wenchuan earthquake, China, and its mechanism (in Chinese with English Abstract). *Seismol. Geol.* 35 (2), 14.

Wang, H., Liang, M. J., Gao, S. P., Ran, Y. K., Chen, L. C., et al. (2018). Reevaluation of coseismic surface ruptures produced by the 1850 M 7.5 Xichang earthquake on the southeastern margin of the Tibetan plateau and implications for rupture propagation at bends on strike-slip faults. *Bull. Seismol. Soc. Am.* 108 (1), 101–115. doi:10.1785/0120170202

Wang, H., Ran, Y. K., Chen, L. C., Liang, M. J., Gao, S. P., and Li, Y. B. (2018). Determination of slip rate on the southern segment of the Aninghe fault (in Chinese with English Abstract). *Seismol. Geol.* 040 (005), 967–979.

Wang, H., Ran, Y. K., Li, Y. B., Gomez, F., and Chen, L. C. (2014). A 3400-year-long paleoseismologic record of earthquakes on the southern segment of Anninghe fault on the southeastern margin of the Tibetan Plateau. *Tectonophysics* 268, 206–217. doi:10.1016/j.tecto.2014.04.040

Wang, X. M. (1992). Discussion on the characteristics and conditions of tectonic rupture of the Xiaojin earthquake (in Chinese). *Sichuan Earthq.* 4, 24–32.

Wang, X. M., and Pei, X. Y. (1998). Some new points of view on the 1786 earthquake (M = 73/4) occurring in the area between KangDing and Moxi, Luding, Sichuan Province (in Chinese). *Earthq. Res. China* 1, 110–117.

Wells, D. L., and Coppersmith, K. J. (1994). New empirical relationships among magnitude, rupture length, rupture width, rupture area, and surface displacement. *Bull. Seismol. Soc. Am.* 84 (4), 974–1002.

Wen, X. Z. (2000). Character of rupture segmentation of the xianshuihe-aninghe-zemuhe fault zone, wester Sichuan (in Chinese with English Abstract). *Seismol. Geol.* 22 (3), 239–249.

Wen, X. Z., Allen, C. R., and Luo, Z. L. (1989). Segmentation, geomrtric features,and their seismotectionic implications for the Holocene Xianshuihe fault zone (in Chinese). *Acta Seismol. sin.* 11 (4), 362–372.

Wen, X. Z., Fang, J., Yi, G. X., Deng, Y. W., and Long, F. (2008). The seismic gap of Aninghe fault in the west of Sichuan (in Chinese). *Sci. China Ser. D Earth Sci.* 22 (3), 239–249.

Xu, X. W., Wen, X. Z., and Zhen, R. Z. (2003). The latest tectonic deformation style and its dynamic source of the active blocks in the Sichuan-Yunnan region (in Chinese with English Abstract). *Sci. China (series D)*, 12–20.

Yuan, Z. D. (2018). *Long paleoseismic record on the wuzunxiaoer-xorkoli section of the central Altyn Tagh fault*. Ph.D. Thesis. China Earthquake Administration: Institute of Geology. (in Chinese with English Abstract).

Zhang, P. Z., Deng, Q. D., Zhang, G. M., Ma, J., Gan, W. J., Min, W., et al. (2003). China continental strong earthquake activities and active blocks (in Chinese). *Sci. China Ser. D. Earth Sci.* 33, 12–20.

Zhao, G. G., Liu, D. Q., and Wei, W. (1990). "The late Quaternary slip rate and segmentation of the Xianshuihe active fault zone," in Proceedings of the PRC-USA bilateral symposium on the Xianshuihe fault zone (Seismological Press Beijing), 41–57.

Zhou, R. J., He, Y. L., Yang, T., He, Q., and Li, X. G. (2001a). Slip rate strong earthquake rupture on the Moxi-Manning segment along the Xianshuihe-Aninghe fault zone (in Chinese). *Earthq. Res. Chian* 17 (03), 253–262.

Zhou, R. J., He, Y. L., Yang, T., He, Q., and Li, X. G. (2001b). Slip rate and strong earthquake rupture on the Moxi—Mianning segment along the xianshuihe-anninghe fault zone (in Chinese). *Earthq. Res. China* 17 (3), 25–34.